

AperTO - Archivio Istituzionale Open Access dell'Università di Torino

## Relative energy of Aluminium Hydroxides: the role of electron correlation.

### This is the author's manuscript

*Original Citation:*

*Availability:*

This version is available <http://hdl.handle.net/2318/124277> since 2016-08-16T11:48:06Z

*Published version:*

DOI:10.1021/jp300419t

*Terms of use:*

Open Access

Anyone can freely access the full text of works made available as "Open Access". Works made available under a Creative Commons license can be used according to the terms and conditions of said license. Use of all other works requires consent of the right holder (author or publisher) if not exempted from copyright protection by the applicable law.

(Article begins on next page)

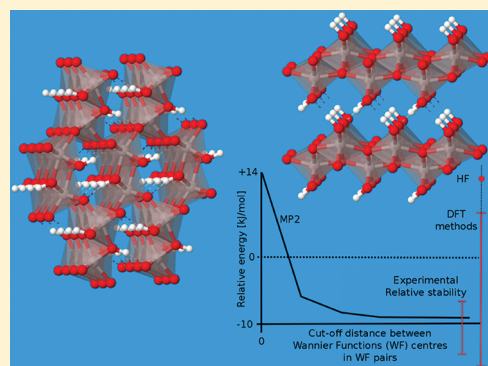
# 1 Relative Energy of Aluminum Hydroxides: The Role of Electron 2 Correlation

3 Silvia Casassa<sup>\*,†</sup> and Raffaella Demichelis<sup>‡</sup>

4 <sup>†</sup>Dipartimento Chimica IFM and Centre of Excellence NIS (Nanostructured Interfaces and Surfaces), Università degli Studi di  
5 Torino, via P. Giuria 5, I-10125 Torino, Italy

6 <sup>‡</sup>Nanochemistry Research Institute, Department of Chemistry, Curtin University, GPO Box U1987, Perth, WA 6845, Australia

7 **ABSTRACT:** The relative energy of aluminum mono- (boehmite and  
8 diaspore) and trihydroxides (gibbsite, bayerite, doyleite, and nordstrandite)  
9 was investigated with a periodic local Møller–Plesset second-order  
10 perturbative approach, with the aim of providing a reliable trend of stability  
11 on the basis of a proper description of both the long-range Coulomb  
12 interactions and the short-range correlation effects. These components,  
13 disregarded in previous studies based on the density functional theory, turn  
14 out to be important for these kinds of systems, where hydrogen bonds and van  
15 der Waals forces play a fundamental role in stabilizing the structure. The  
16 results are in good agreement with the available experimental evidence. The  
17 reasons for the monohydroxides energy difference were investigated, with  
18 diaspore showing an electronic structure for oxygen atoms more favorable  
19 than that for boehmite. The problem of the nordstrandite structure was re-  
20 examined because of the presence of a second minimum energy structure on  
21 the energy surface. Both of them are higher in energy than those of the other trihydroxide polymorphs, and the relative stability  
22 of one of these structures with respect to gibbsite is in agreement with recent experimental investigations.



## 1. INTRODUCTION

23 Aluminum mono- and trihydroxides exhibit the general formula  
24  $\text{Al}_2\text{O}_3 \cdot n\text{H}_2\text{O}$ , where  $n = 1$  for monohydroxides (boehmite and  
25 diaspore), and  $n = 3$  for trihydroxides (bayerite, gibbsite,  
26 nordstrandite, and doyleite). They all consist of an oxygen  
27 network with Al hosted in interstices and octahedrally  
28 coordinated. Hydrogen bonds (HB) are present, which ensure  
29 the interlayer cohesion of layered structures (all but diaspore).  
30 Gibbsite (indicated as  $\mathcal{G}$  in the following), boehmite ( $\mathcal{Bh}$ )  
31 and diaspore ( $\mathcal{Ds}$ ) are the main constituents of aluminum ores.  
32 Bayerite ( $\mathcal{By}$ ) is less abundant, whereas doyleite ( $\mathcal{Dy}$ ) and  
33 nordstrandite ( $\mathcal{N}$ ) are rarely observed as natural compounds.  
34 They all play an important role in the aluminum industry, as  
35 hydrated precursor of transition aluminas or as raw materials  
36 for the manufacture of many objects, other than being used also  
37 as adsorbents, emulsifiers, ion exchangers, antacid drugs, and  
38 filtering media.<sup>1–6</sup>

39 Despite several experimental studies carried out during the  
40 last 50 years, some of their properties are still a matter of  
41 debate, due to the many problems affecting the experimental  
42 measures (e.g., adsorbed water, disorder, mixed phases,  
43 environment pH) and thus giving rise to different interpreta-  
44 tions by the various authors.<sup>7</sup>

45 In the past few years some of the unresolved questions have  
46 been addressed to atomistic simulation, the main outcomes  
47 being the unambiguous determination of the structure and the  
48 HB pattern,<sup>7–13</sup> the accurate analysis of the vibrational  
49 properties,<sup>7–9,14–17</sup> and the study of boehmite surface and

water-surface properties.<sup>18,19</sup> Less successful results were  
50 obtained when trying to estimate the energetics at the density  
51 functional theory level (DFT),<sup>7,12,20–24</sup> the worst case being  
52 the relative stability between boehmite and diaspore, shown to  
53 be functional-dependent due to their major structural differ-  
54 ences.<sup>7,24</sup>

55 Thermodynamic properties represent a mandatory item for a  
56 better insight into the physical chemistry of aluminum  
57 hydroxides and a step for further investigations of the structure  
58 of transition aluminas. When considering the relative stability of  
59 aluminum hydroxides in a wide range of temperatures, the  
60 following framework emerges from the most accredited  
61 experiments and simulations: (i) the lower the temperature,  
62 the higher the hydration degree; (ii) the HB pattern might be  
63 one of the main responsible for the energy difference of the  
64 polymorphs; for trihydroxides, the stacking sequence of the  
65 layers, which can determine a more convenient HB pattern in  
66 terms of  $\text{H}\cdots\text{O}$  and  $\text{O}-\text{H}$  distances and  $\text{O}-\text{H}\cdots\text{O}$  angles, was  
67 shown to have a non-negligible effect in determining the  
68 relative stability of the polymorphs;<sup>12,13</sup> (iii)  $\mathcal{Ds}$  and  $\mathcal{G}$  are  
69 considered the most stable mono- and trihydrated phases at  
70 standard conditions, respectively.

71 However, many contradictions are present in the literature,  
72 and quantitative values are still missing. In the case of 73

Received: January 13, 2012

Revised: April 16, 2012

trihydroxides, only data for  $\mathcal{B}y$  and  $\mathcal{G}$  are available, with  $\Delta G^{298}$ , i.e., the Gibbs free energy difference between the two compounds, ranging from  $-11.8$  to  $-4.0$  kJ/mol per  $\text{Al}_2\text{O}_3$  unit<sup>1,25–27</sup> (with error bars between  $\pm 1$  and  $\pm 8$  kJ/mol and  $\mathcal{G}$  being the most stable). Clear experimental evidence is not yet available for  $\mathcal{D}y$  and  $\mathcal{N}$ , and contrasting data were proposed as a result of a DFT simulation<sup>7</sup> and Hemingway and Sposito's estimations.<sup>28</sup>

Because of the high structural similarity of these four polymorphs, their relative stability is quite well reproduced with DFT simulations (i.e., roughly, they are affected by the same error in estimating interlayer dispersive interactions):  $\Delta G^{298}$  between  $\mathcal{B}y$  and  $\mathcal{G}$  ranges from  $-10.3$  to  $-5.8$  kJ/mol with six different functionals.<sup>24</sup>  $\Delta G^{298}$  between  $\mathcal{N}$  or  $\mathcal{D}y$  and  $\mathcal{G}$  obtained with three different levels of DFT approximation ranges from  $-30.3$  to  $-27.5$  kJ/mol and from  $-10.6$  to  $-8.8$  kJ/mol,<sup>7</sup> respectively, whereas Hemingway and Sposito<sup>28</sup> estimated it to be  $-6.8$  and  $-8.8$  kJ/mol, respectively. Recently, thermochemical experiments have been carried out on  $\mathcal{N}$ , estimating its enthalpy difference with respect to  $\mathcal{G}$ ,  $\Delta H^{298}$ , to  $-28.2 \pm 3.6$  kJ/mol.<sup>29</sup> Assuming the similarity of standard entropies of the two polymorphs, this datum can be roughly compared to the results of the previous DFT simulations,<sup>7,13</sup> showing a good agreement and thus confirming the high instability of  $\mathcal{N}$  with respect to its polymorphs.

Concerning monohydroxides, the experimental  $\Delta G^{298}$  between  $\mathcal{B}h$  and  $\mathcal{D}s$  ranges from  $-15.5$  to  $-6.7$  kJ/mol per  $\text{Al}_2\text{O}_3$  unit<sup>1,25–27</sup> (with error bars between  $\pm 5$  and  $\pm 13$  kJ/mol and  $\mathcal{D}s$  being the most stable). DFT simulations provide  $\Delta G^{298}$  data from  $-16.2$  to  $+7.5$  kJ/mol,<sup>22,24,30</sup> depending on the adopted method (level of approximation, basis set, and pseudopotential). This is probably due to the major structural differences between  $\mathcal{B}h$  and  $\mathcal{D}s$ , in particular to the layered nature of  $\mathcal{B}h$ , and a significant improvement in the results could be obtained with a more accurate estimation of both exchange and Coulomb electron correlation.

In this paper, we used a quantum-mechanical periodic local<sup>31–33</sup> Møller–Plesset perturbative approach truncated at the second order (LMP2), as implemented in the CRYSCOR code,<sup>34,35</sup> for the study of aluminum mono- and trihydroxides. The aims are to provide unambiguous data for their relative energy and to demonstrate the effectiveness of this post-Hartree–Fock (HF) scheme for the treatment of electron correlation in large unit cell systems containing different chemical bonds (covalent, semi-ionic, HB) to be described with the same accuracy and non-negligible van der Waals interactions.

The paper is structured as follows. Section 2 deals with the adopted computational methods, focusing on the accurate calibration of parameters and basis set for the LMP2 calculations. Results are reported, discussed, and compared with DFT and experimental data in section 3, where the analysis of the LMP2 energy contribution is also performed. Finally, section 4 summarizes the main conclusions.

## 2. COMPUTATIONAL METHODS

These calculations were performed with the periodic ab initio CRYSTAL09<sup>36</sup> and CRYSCOR09<sup>37,38</sup> codes, using all electron Gaussian-type basis sets. Because an automatic procedure for the analytical geometry optimization at the LMP2 level is not yet available in CRYSCOR, equilibrium geometries were obtained at the DFT (SVWN,<sup>39,40</sup> PBE,<sup>41</sup> PBEsol,<sup>42</sup> PBE0,<sup>43</sup>

and B3LYP<sup>44,45</sup>) and HF levels, with 8-621G(d) (Al), 8-411G(d) (O), and 211G(p) (H) basis sets,<sup>17</sup> indicated in the following as BSA. Geometry optimization was performed using analytical gradients with respect to atomic coordinates and unit-cell parameters, within a quasi-Newtonian scheme combined with Broyden–Fletcher–Goldfarb–Shanno<sup>46–49</sup> Hessian updating. The default convergence criteria were used for both gradient components and nuclear displacements. The phonon spectra were computed by diagonalizing the dynamical matrix built by numerically differencing the analytical gradient with respect to atomic Cartesian coordinates. Tolerances on the self-consistent field were set to  $10^{-8}$  a.u. for geometry optimization and to  $10^{-10}$  a.u. for frequency calculation. The DFT exchange–correlation contribution was evaluated by numerical integration over the unit cell volume, using a pruned grid with 75 radial (Gauss–Legendre radial quadrature) and 974 angular (Lebedev two-dimensional generation) points.

To properly compare our results with experimental data, the electronic energy obtained with the LMP2 approach should be corrected by the zero point energy, the entropy, and the heat capacity at 298 K. However, the fact that the phonon calculation is not yet implemented in CRYSCOR is only a minor limit for this study, because vibrational contributions to the free energy of these systems are on the order of 1–2 kJ/mol per  $\text{Al}_2\text{O}_3$  unit with all the adopted DFT schemes, much smaller than the experimental error bar, and were shown to be insufficient to invert the stability between these polymorphs.<sup>24</sup>

The five parameters controlling the Coulomb and HF exchange series accuracy were set to [7,7,7,16] and, once the equilibrium structure was obtained, were tightened to [7,7,7,15,50] for the evaluation of the high-quality one-electron HF wave functions required by the post-HF correction.<sup>36</sup> The reciprocal space was sampled using a shrinking factor  $IS = 8$  for monohydroxides (i.e., 105 k points in the irreducible part of the Brillouin zone for  $\mathcal{B}h$  and 125 for  $\mathcal{D}s$ ) and  $IS = 6$  for trihydroxides (80 k points for  $\mathcal{G}$  and  $\mathcal{B}y$  and 112 for  $\mathcal{D}y$  and  $\mathcal{N}$ ). The same grids were adopted in the unitary transformation of the crystalline orbitals yielding the equivalent set of well-localized, symmetry adapted, mutually orthogonal, translationally equivalent Wannier functions<sup>50,51</sup> (WF) used to describe the valence part of the occupied manifold in CRYSCOR.

**Calibration of LMP2 Computational Parameters.** The size of trihydroxides (192 valence electrons for  $\mathcal{G}$  and  $\mathcal{B}y$ ), which currently represents an upper limit for the CRYSCOR code in terms of memory usage and CPU time, and the relatively small energy difference between polymorphs are such that computational parameters must be accurately set, to achieve a compromise between good results quality and reasonable computational effort.

Starting from the geometry optimized at the PBE0 level (shown in previous works<sup>24,52</sup> to provide very small deviation from experimental structures at 298 K), the LMP2 contribution to the relative energy between  $\mathcal{D}s$  and  $\mathcal{B}h$  (64 and 32 valence electrons, respectively),  $\Delta E_{\text{mono}}^{(2)}$ , was evaluated adopting (a) different locality truncation tolerances and (b) different basis sets.

**a. Locality Truncation Tolerances.** The complete treatment of the periodic LMP2 approach, as implemented in the CRYSCOR code, is reported in ref 53. Let us briefly fix the notation and introduce the main computational parameters of the LMP2 calculation. As already anticipated, WFs ( $\{\omega\}$ ) play an essential role in CRYSCOR, together with the complementary set of projected atomic orbitals (PAO,  $\{\chi\}$ ) which

span the virtual space. Both these sets of functions are translationally equivalent, so that it is possible to define the reference ones (indexed  $i, j, \dots$  and  $a, b, \dots$ ) settled in the reference zero cell and then concisely indicate the others according to the crystalline cell ( $I, J, \dots$  and  $A, B, \dots$ ) they belong to as  $\omega_{iI}, \omega_{jJ}, \dots$  and  $\tilde{\chi}_{aA}, \tilde{\chi}_{bB}, \dots$ , respectively. Adopting the close notation  $J \equiv jJ$ ,  $A \equiv jA$  and being the first WF always in the reference cell,  $I \equiv iI \equiv i0 \equiv i$ , the LMP2 energy  $E^{(2)}$  can be written as a sum of all contributions  $E_{ij}^{AB}$

$$E^{(2)} = \sum_{i \in \text{cell}} \sum_{d_{ij} < d} E_{ij}^{(2)} \quad (1)$$

$$\begin{aligned} E_{ij}^{(2)} &= \sum_{(A,B) \in (i,J)} E_{ij}^{AB} \\ &= \sum_{(A,B) \in (i,J)} K_{AB}^{ij} (2T_{AB}^{ij} - T_{BA}^{ij}) \end{aligned} \quad (2)$$

each corresponding to a two-electron excitation from a pair of WFs (WW pair) to a pair of PAOs,  $[(ij) \uparrow \uparrow (AB)]$ .  $K_{AB}^{ij}$  are the electron repulsion integrals between the WF-PAO product distribution and  $T_{AB}^{ij}$  are the excitation amplitudes calculated via a self-consistent procedure.

The input parameters serve essentially to fix three kinds of tolerances, all concerning the treatment of WFs and PAOs. The first one determines the truncation of their tails: in the linear combinations defining WFs and PAOs, atomic orbitals (AOs) with coefficients lower than  $t$  (default  $t = 0.0001$  was used) are disregarded.

The other two parameters are used to exploit the local-correlation Ansatz according to which all excitations can be ignored except those involving close-by WF and PAO pairs: a domain  $D_i$  is associated to the general WF ( $\omega_i$ ), consisting of a certain number of atoms close to it. Two WFs then define a pair-domain  $D_{(ij)}$  which is simply the union of the corresponding domains. Only excitations  $[(ij) \uparrow \uparrow (AB)]$  for which both PAOs  $A$  and  $B$  belong to atoms in  $D_{(ij)}$  and the distance  $d_{ij}$  between the centers of the two WFs is within a certain value  $d$  are retained (see notations  $d_{ij} < d$  in eq 1 and  $(A,B) \in (i,J)$  in eq 2). The contributions due to WW pairs further than  $d$  are not explicitly evaluated but can be estimated a posteriori by means of an extrapolation technique, which exploits the fact that pair correlation energies asymptotically decrease with distance between electron according to the London  $ar^{-6}$  law<sup>54</sup> (LJ).

Figure 1 reports the difference between  $\Delta E_{\text{mono}}^{(2)}(d)$  and the extrapolated limit  $\Delta E_{\text{mono}}^{(2)}(\infty)$  as a function of  $d$ : the expected  $d^{-3}$  behavior of the difference is observed, and the extrapolation procedure appropriately corrects for the missing contributions. A value of  $d = 12$  Å, combined with the systematic use of the LJ technique, was set.

Regarding the third local parameter, namely the PAOs selection, the Boughton–Pulay criterion with a value of 0.985 was used, which corresponds for all the polymorphs to an average number of atoms  $n_\alpha = 4$  for each  $D_i$ . Domains with  $n_\alpha$  ranging from 2 to 14 were tested but, in contrast to a quadratically increase of computing time and memory usage, the difference when passing from  $n_\alpha = 4$  to  $n_\alpha = 14$  is on the order of 10  $\mu$ Hartree.

**b. Basis Set.** Basis set incompleteness is a principal problem for an accurate post-HF calculation, where diffuse high angular momentum functions are required to properly describe the

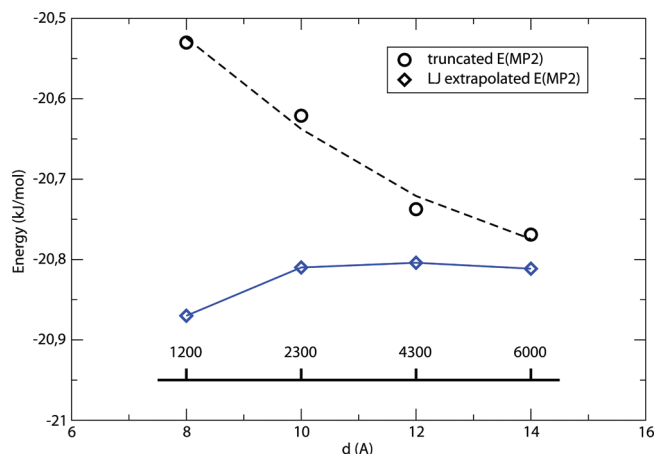


**Figure 1.** Correlation energy difference between  $\mathcal{D}$ s and  $\mathcal{B}h$ ,  $\Delta E_{\text{mono}}^{(2)}$  (kJ/mol per  $\text{Al}_2\text{O}_3$ ), as a function of the cutoff distance  $d$  between WW pairs (the number of pairs included in eq 1 is reported on the straight line). Circles are the uncorrected values, and diamonds are the corrected ones for the London extrapolation. Geometries optimized at the PBE0 level, BSA basis set.

Coulomb hole. However, basis sets richer than BSA are not suitable to trihydroxides with CRYSCOR, because of the size of the systems.

To verify the accuracy of the results obtained with BSA, the effect of the basis set on  $\Delta E_{\text{mono}}^{(2)}$  was tested. Two basis sets, namely BSB and BSC, were refined starting from BSA, with the exponents of the outermost shells taken from the standard cc-pVTZ set of Dunning.<sup>55,56</sup> In particular, BSB was obtained from BSA by adding an f shell to the O atom ( $\alpha_f = 1.428$ ). BSC was obtained from BSB by splitting the d shell of the O atom (from  $\alpha_{\text{d,BSB}} = 0.45$  to  $\alpha_{\text{d1,BSC}} = 2.31$ ,  $\alpha_{\text{d2,BSC}} = 0.645$ ), adding an f shell to the Al atom ( $\alpha_f = 0.244$ ) and modifying its d exponent (from  $\alpha_{\text{d,BSB}} = 0.6$  to  $\alpha_{\text{d,BSC}} = 0.33$ ). Results for  $\Delta E_{\text{mono}}^{(2)}$  in kJ/mol per  $\text{Al}_2\text{O}_3$  unit are  $-8.84$ ,  $-9.03$ , and  $9.46$  for BSA, BSB, and BSC, respectively.

Despite its poor quality for a routinely LMP2 calculation, BSA allows for a sufficiently accurate comparison of the considered systems, with a difference on total energy around 6% with respect to BSC. This is not totally surprising because the error affecting energies due to basis set incompleteness is approximately constant and cancel almost exactly when differences among similar systems are considered.

### 3. RESULTS

**A. LMP2 Relative Energies.** As anticipated, the full geometry relaxation scheme at the LMP2 level is not yet implemented in the adopted code, and equilibrium geometries obtained by means of HF and different DFT approaches were considered as a starting point for the HF+LMP2 calculation.

Let us first concentrate on the monohydrated polymorphs.  $\mathcal{D}$ s and  $\mathcal{B}h$  are very different forms of the same compound, the former being a dense nonlayered structure (volume per formula unit 9% smaller than that of  $\mathcal{B}h$ ) and the latter being a stacking of layers kept together by HBs and dispersive forces. Both polymorphs exhibit relatively strong HBs ( $\text{H}\cdots\text{O}$  1.7 Å), either contained in small cavities ( $\mathcal{D}$ s), or pointing toward the adjacent layers ( $\mathcal{B}h$ ).

In the case of DFT methods, a general evidence of the correlation between structural predictions and relative energies was found.<sup>24</sup> In particular, functionals underestimating the



volume tend to overstabilize the denser structure and vice versa, the exception being GGA functionals recently reparametrized for solids (i.e., PBEsol), which turned out to provide at least the correct stability order for the considered systems. This implies that every time polymorphs with very different structures are compared, as is the case of monohydroxides, very different and conflicting results can be obtained depending on the adopted functional.

The main reason for such a wide range of results for Al monohydroxides ( $\Delta E_{\text{mono}}$  from  $-18$ , with SVWN, to  $+4.5$ , with B3LYP, kJ/mol per  $\text{Al}_2\text{O}_3$ , see Tables 1 and 2 and ref 24) might

**Table 1. Relative Energy (kJ/mol per  $\text{Al}_2\text{O}_3$ ) between  $\mathcal{D}_s$  and  $\mathcal{B}h$  Evaluated with BSA and BSC, Using Equilibrium Geometries Obtained with Different DFT Functionals and BSA Basis Set<sup>a</sup>**

geometry	$\Delta E_{\text{mono}}^{\text{HF}}$		$\Delta E_{\text{mono}}^{(2)}$		$\Delta E_{\text{mono}}$	
	BSA	BSC	BSA	BSC	BSA	BSC
SVWN	3.3	1.8	-12.7	-13.7	-9.4	-11.9
PBE	10.1	9.1	-22.2	-21.8	-12.0	-12.7
PBEsol	7.9	6.8	-19.7	-19.6	-11.8	-12.7
PBE0	12.0	10.1	-20.8	-19.6	-8.8	-9.5
B3LYP	11.3	9.0	-16.3	-17.8	-5.0	-8.8
HF	13.1	12.2	-19.7	-20.5	-6.6	-8.3

<sup>a</sup>HF ( $\Delta E_{\text{mono}}^{\text{HF}}$ ) and LMP2 ( $\Delta E_{\text{mono}}^{(2)}$ ) contributions to the total energy ( $\Delta E_{\text{mono}}$ ) are shown separately.

**Table 2. Relative Energies (kJ/mol per  $\text{Al}_2\text{O}_3$ ) for Mono- And Trihydroxides at the DFT and LMP2 Levels<sup>a</sup>**

	$\Delta E_{\text{mono}}$	$\Delta E_{\mathcal{G}-\mathcal{B}y}$	$\Delta E_{\mathcal{G}-\mathcal{D}y}$	$\Delta E_{\mathcal{G}-\mathcal{N}}$
SVWN	-18.1	-10.6	-9.25	-28.9 (ST1)
PBE	-0.5	-7.7	-9.72	-28.8 (ST1)
PBEsol	-10.5	-11.4	-9.88	-28.8 (ST1)
B3LYP	4.5	-9.6	-8.28	-29.8 (ST1)
B3LYP	—	—	—	-17.6 (ST2)
PBE0	1.0	-7.2	-8.82	-16.6 (ST2)
LMP2(PBE)	-12.0	-4.3	-8.6	-27.5 (ST1)
LMP2(B3LYP)	-5.0	-5.9	-10.7	-29.7 (ST1)
LMP2(B3LYP)	—	—	—	-13.8 (ST2)
LMP2(PBE0)	-8.8	-5.1	-8.5	-12.8 (ST2)
$\Delta G_{298}^{\text{exp}}$	-6.7/-15.5	-4.0/-11.8	—	—
$\Delta H_{298}^{\text{exp}}$	—	—	—	-28.2

<sup>a</sup>BSA was used. LMP2 data were obtained for PBE, B3LYP and PBE0 geometries. ST1 and ST2 refer to the structure of  $\mathcal{N}$ , see text for details. Experimental Gibbs free energy difference,  $\Delta G_{298}^{\text{exp}}$ , from refs 1, 25–27, and enthalpy difference,  $\Delta H_{298}^{\text{exp}}$ , from ref 29.

be the incorrect evaluation of van der Waals and dispersive forces between  $\mathcal{B}h$  layers by the various DFT functionals. This would be a minor effect if both compounds were layered structures with similar features (as in the case of trihydroxides; see later on), because the error would cancel nearly exactly when computing the energy difference.

When performing the HF calculation starting from the various equilibrium geometries,  $\mathcal{B}h$  is predicted as the lowest energy structure. As expected, also the HF approximation is unable to describe properly the long-range dispersive interactions that, on the basis of the correlated-corrected results, are responsible for the opposite observed relative energy. As a matter of fact, in all the considered cases, the LMP2 contribution inverts the relative energy of the two phases

predicting  $\mathcal{D}_s$  more “stable” than  $\mathcal{B}h$  by 8.3–12.7 kJ/mol (see Table 1). For an appropriate use of the term “stability” and a direct comparison to the experimental data, one might include the thermodynamic contributions in the estimation. However, for these systems they were shown to contribute by about 1–2 kJ/mol to the Gibbs energy with several DFT functional,<sup>7,52</sup> so that we can assume that our current results are reasonable and in agreement with the experimental range of stability.

The extension of this approach to the study of trihydroxides supports our considerations. As anticipated, the large unit cell of  $\mathcal{B}y$  and  $\mathcal{G}$  is currently a limit for the adopted code, so that BSA was used. LMP2 relative stabilities of  $\mathcal{B}y$ ,  $\mathcal{D}y$  and  $\mathcal{N}$  with respect to  $\mathcal{G}$ , starting from equilibrium geometries evaluated at different DFT levels, are reported in Table 2. The relative energy of monohydroxides calculated with the same basis set is also reported for the sake of comparison.

As expected, the LMP2 contribution to the total energy is not as crucial as for the monohydroxides in deciding the relative energies of trihydroxides, because of their very similar structural features. However, there are a few concerns regarding  $\mathcal{N}$ . Unfortunately, only a couple of dated experimental studies are available for this structure, and their accuracy is very poor. Moreover, no experimental data regarding the H atom positions and the HB pattern are available. A solution to the  $\mathcal{N}$  structural problem was proposed as a result of first principles calculations at the B3LYP level in ref 13, in good agreement with the experimental structure proposed by Saalfeld and Jarchow<sup>57</sup> and confirmed later by Chao and Baker.<sup>58</sup> The same structure was shown to exhibit vibrational features in good agreement with experimental IR and Raman spectra in ref 7. Also, its relative stability with respect to  $\mathcal{G}$  has been recently confirmed by thermochemical experiments.<sup>29</sup>

When optimizing the structure with SVWN, PBEsol, and PBE, results similar to that with B3LYP were provided, whereas with PBE0 a quite different and much more stable structure was obtained. Phonon calculation confirmed that this is a minimum energy structure, and the optimizations with the other functionals using the new structure as an initial guess (instead of the experimental one) all led to a similar result.

Table 3 shows the experimental structure, those optimized with B3LYP and PBE0 using the experimental parameters as an initial guess, and that obtained with B3LYP using the PBE0 result as an initial guess. The main differences between the less stable and the more stable structures (in the following ST1 and ST2, respectively) are related to the stacking of the layers, i.e., the  $c$  and  $\alpha$  lattice parameters (differing by 9–15% with respect to the experimental structure), whereas the geometry within a single layer is preserved. This modification also involves the HB pattern, shown in table 4. Both structures exhibit quite unusual O–H...O angles and relatively long HBs with respect to the other Al hydroxides, but the interlayer setting of ST2 allows the formation of stronger HB interactions (1.853 Å), which is probably one of the main responsible for the stabilization of this structure.

Dealing with the  $\mathcal{N}$  structure and, in general, with the possible arrangements of  $\text{Al}(\text{OH})_3$  layers is not the purpose of this paper, so we do not enter into further detail. The only comment we add is that the available experimental evidence (structural, vibrational, and thermochemical) suggests ST1 as the best candidate for the  $\mathcal{N}$  structure. However, considering that a new minimum energy structure was obtained (ST2) and that, despite exhibiting the largest deviation from the experimental geometry, it turns out to be around 15 kJ/mol

**Table 3. Structure of  $\mathcal{N}$ : Experimental Data, PBE0 and B3LYP Results (ST2 and ST1, respectively) Obtained Using the Experimental Structure as an Initial Guess, and B3LYP Results (ST2) Obtained Using the PBE0 Structure As Initial Guess<sup>a</sup>**

	exp <sup>57</sup>	B3LYP (from exp)	PBE0 (from exp)	B3LYP (from PBE0)
<i>a</i>	5.069	5.056	4.988	5.039
<i>b</i>	8.752	8.868	8.804	8.895
<i>c</i>	6.155	6.296	5.320	5.371
$\alpha$	127.73	127.70	115.59	114.28
$\beta$	80.97	81.39	82.44	81.63
$\gamma$	91.66	88.98	90.24	90.44
vol	212.48	218.64	208.49	216.76
Al–O <sub>max</sub>	2.041	1.955	1.923	1.935
Al–O <sub>min</sub>	1.821	1.882	1.884	1.894
O–H <sub>max</sub>	–	0.978	0.979	0.978
O–H <sub>min</sub>	–	0.968	0.964	0.966
H···O <sub>max</sub>	–	2.257	2.362	2.232
H···O <sub>min</sub>	–	1.914	1.792	1.853
O–H···O <sub>max</sub>	–	176.5	168.9	170.9
O–H···O <sub>min</sub>	–	140.2	136.5	138.7
$\Delta E$	–	–29.79	–16.59	–17.59

<sup>a</sup>The relative energy with respect to  $\mathcal{G}$  ( $\Delta E$ , kJ/mol per  $\text{A}_2\text{O}_3$ ) is reported. Lengths in angstroms, angles in degrees; BSA was used.

**Table 4. Hydrogen Bond Pattern in ST1 and ST2 As Obtained with the B3LYP Functional and BSA<sup>a</sup>**

	ST1				ST2			
	O–H	H···O	type	O–H···O	O–H	H···O	type	O–H···O
(O–H) <sub>(1)</sub>	0.968	1.994	inter	150.9	0.966	2.157	inter	138.9
(O–H) <sub>(2)</sub>	0.978	1.914	inter	176.5	0.976	1.924	inter	170.9
(O–H) <sub>(3)</sub>	0.972	1.982	inter	166.6	0.978	1.853	inter	165.2
(O–H) <sub>(4)</sub>	0.977	2.018	intra	150.5	0.972	2.226	intra	142.7
(O–H) <sub>(6)</sub>	0.973	2.257	intra	140.2	0.973	2.232	intra	142.8
(O–H) <sub>(5)</sub>	0.968	(2.322–2.329)	1,3(intra)	(93.5, 105.1)	0.9658	(2.465–2.581)	(inter-intra)	(111.7–92.0)

<sup>a</sup>Lengths in angstroms, angles in degrees. Intra and inter refer to intralayer and interlayer HB interaction, respectively.

more stable than ST1, the corresponding fractional coordinates of the asymmetric unit are reported in Table 5. Whichever the

**Table 5. Fractional Coordinates of the ST2 Structure Optimized with B3LYP and BSA**

	<i>x/a</i>	<i>y/b</i>	<i>z/c</i>
Al	0.02066	0.33295	0.99047
Al	0.48434	0.83575	0.00615
O	0.25616	0.75290	0.23464
O	0.80608	0.23219	0.20002
O	0.32522	0.05829	0.20825
O	0.83173	0.54179	0.20295
O	0.76178	0.86739	0.22371
O	0.30546	0.36949	0.21058
H	0.19269	0.84483	0.40864
H	0.76065	0.29192	0.39809
H	0.13498	0.06442	0.19687
H	0.79473	0.58358	0.40404
H	0.70353	0.88361	0.41533
H	0.41298	0.46045	0.20937

structure, both the  $\mathcal{N}$  models are much higher in energy than the other Al trihydroxide polymorphs with all the considered functionals, also when the LMP2 correction is included. The stability order of  $\text{Al}(\text{OH})_3$  polymorphs is unambiguously confirmed in this study, with  $\mathcal{G}$  being the lowest energy structure, followed by  $\mathcal{B}_y$  (between +4 and +6 kJ/mol),  $\mathcal{D}_y$

(between +8 and +11 kJ/mol), and  $\mathcal{N}$  (either around +28 kJ/mol for ST1, or around +12 kJ/mol for ST2).

**B. Energy Partition.** Figure 2 reports the relative energy trend of the polymorphs as a function of the cutoff distance between the centers of WFs in WW pairs  $d_{ij} = |\mathbf{C}_i - \mathbf{C}_j|$ . For each pair,  $d_{ij}$  depends on the crystal cell  $\mathbf{J}$  where the second WF is located, because the first one is always centered in the zero reference cell, and its  $E_{ij}^{(2)}$  contribution decreases following the

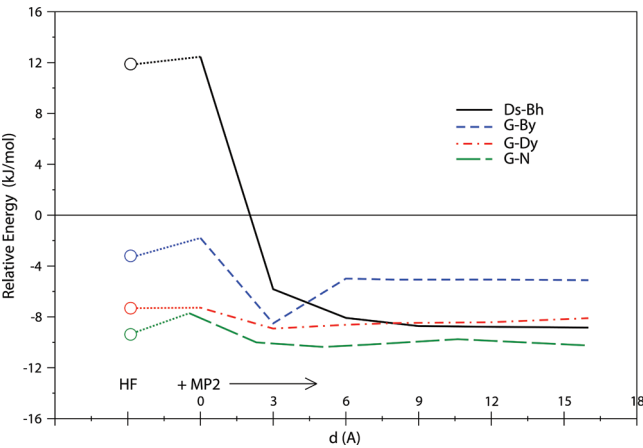


**Figure 2.** Relative energy trend as a function of the cutoff distance between the centers of WW pairs:  $\mathcal{D}_s$  vs  $\mathcal{B}_h$  and  $\mathcal{G}$  vs  $\mathcal{B}_y$ ,  $\mathcal{D}_y$  and  $\mathcal{N}$ . Geometries optimized at the PBE0 level, BSA basis set.

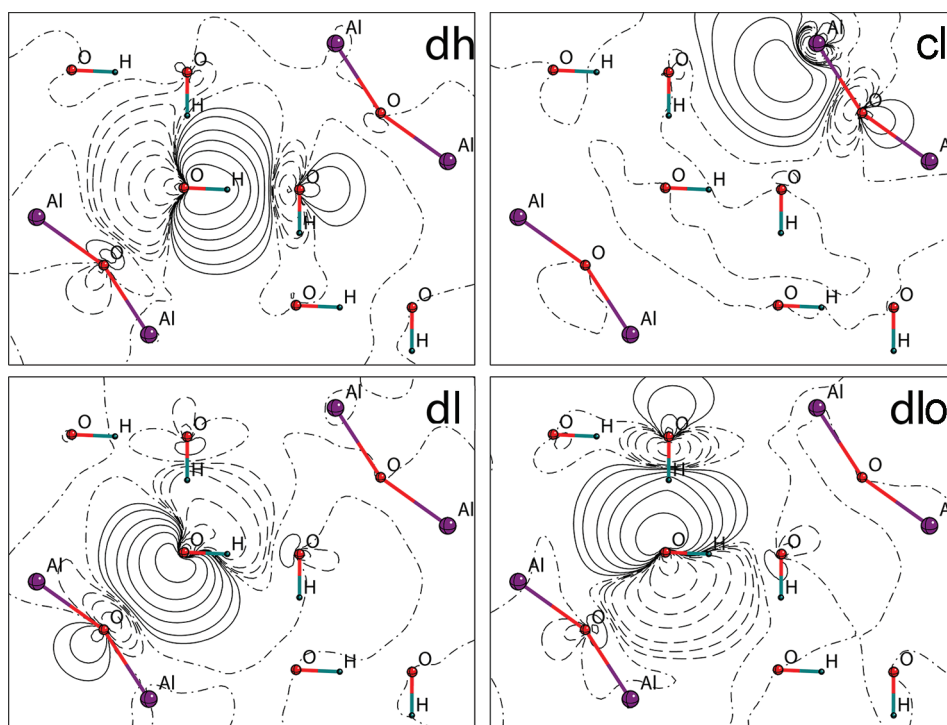


**Figure 3.** Projection of the four types of  $\mathcal{B}h$  WFs:  $\omega_d^h, \omega_c^1, \omega_b^1, \omega_a^{1o}$ . The selected plane permits appreciation of the differences between the  $\omega_d^h, \omega_b^1$  and  $\omega_a^{1o}$  WFs. Isoamplitude lines differ by 0.01 au; positive, zero, and negative amplitudes are drawn with solid, dot-dashed, and dashed lines, respectively.

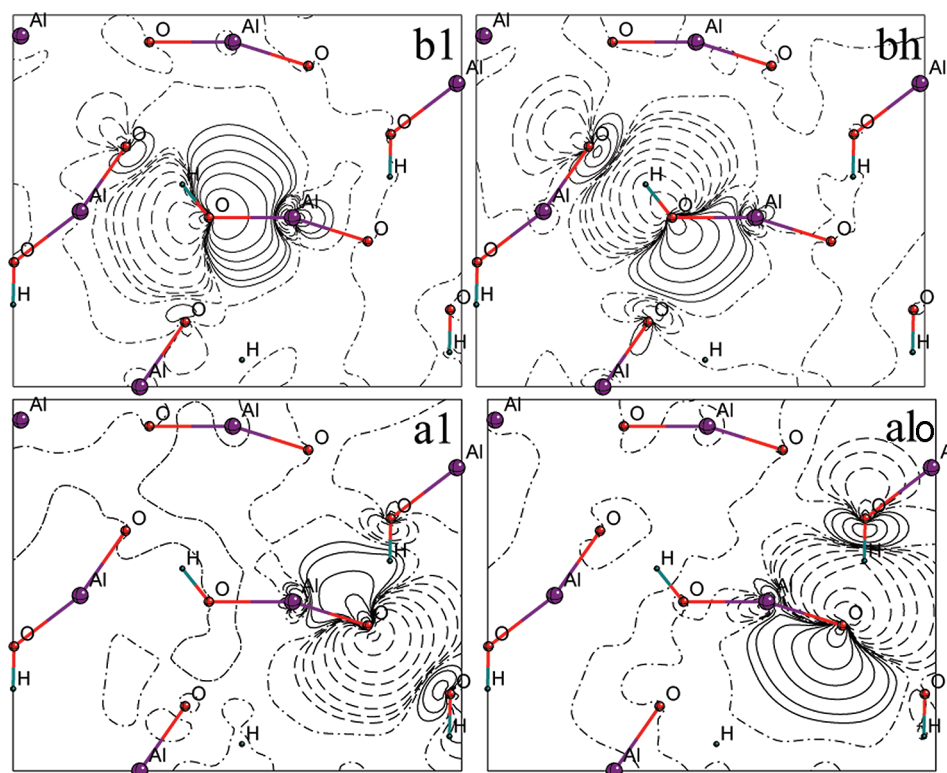


**Figure 4.** Projection of the four types of  $\mathcal{D}s$  WFs:  $\omega_b^1, \omega_b^h, \omega_a^{1o}, \omega_a^1$ . Conventions as in Figure 3.

392  $r^{-6}$  law as  $d_{ij}$  increases.  $\mathcal{D}s$  and  $\mathcal{G}$  are taken as a reference for  
 393 mono- and trihydroxides, respectively. The ST2 structure was  
 394 used for  $\mathcal{N}$ , because of its higher stability with respect to ST1.  
 395 Good results were obtained at the HF and DFT levels for the  
 396 relative energy of trihydroxides. This means on the one hand, as  
 397 discussed in the previous sections, that the similarity of the

structures is such that dispersive contributions cancel nearly  
 exactly when performing the energy difference, and on the  
 other hand that electrostatic interactions play the fundamental  
 role in deciding the stability of these structures, whereas  
 dispersive forces only affect their absolute value.

The LMP2 contribution can be partitioned as follows. First, the correlation due to the closest WW pairs, corresponding to WFs centered on the same atom ( $d = 0$ , usually referred as *strong* pairs), tends to stabilize  $\mathcal{B}y$  and  $\mathcal{N}$  with respect to  $\mathcal{G}$ , whereas the energy difference  $\mathcal{D}y - \mathcal{G}$  remains nearly unchanged. Contributions resulting from pairs included in a sphere of 3 Å around the reference cell (called *weak* pairs) strongly favor  $\mathcal{G}$ , and this tendency is only partially compensated in  $\mathcal{B}y$  by contributions between 3 and 6 Å. The long-range part of the correlation energy contributes approximately the same for all the trihydrates, so that we can consider the same trend up to infinity.

Monohydroxides exhibit a rather different behavior (solid line in Figure 2).  $\mathcal{B}h$  is predicted as the most stable phase by the monodeterminantal HF approach, and the opposite relative energy is due to correlation effects. As for the trihydroxides, the addition of the closest pairs energies to the HF one increases by a small amount the relative energy in favor of  $\mathcal{B}h$ . However, as soon as the contributions from *weak* pairs are taken into account,  $\mathcal{D}s$  becomes more stable and the progressive inclusion of contributions arising from further pairs, up to infinity, reinforces the trend.

The analysis of the various pair energies  $E_{ij}^{(2)}$  contributing to  $E^{(2)}$  in terms of type of WFs ( $\omega_i, \omega_j$ ) from which the two electrons are excited permits a better understanding of the underlying physics. Actually, WFs lend themselves to a rather simple chemical interpretation by allowing an easy and intuitive description of the electronic structure in terms of chemical concepts such as lone pairs and ionic or covalent bonds.

The 32 and 64 valence electrons in the unit cell are described by 16 and 32 WF in  $\mathcal{B}h$  and  $\mathcal{D}s$ , respectively, and for both structures an irreducible set of eight symmetry-adapted WFs<sup>51</sup> can be defined associated with the two inequivalent O atoms in the asymmetric unit. These WFs, whose shape is shown in Figures 3 and 4, can be subdivided according to their chemical character as follows.

In  $\mathcal{B}h$ , the symmetry-inequivalent O atoms are  $O_c$  and  $O_d$ , the former having four Al atoms as first neighbors, and the latter having two Al and 1 H atoms as first neighbors and being an HB acceptor. The WFs associated to  $O_c$  ( $\omega_c^1, \omega_c^2, \omega_c^3, \omega_c^4$ ) show a highly ionic character: they are essentially *atomic* functions centered on  $O_c$  and composed by its p-type valence AOs, oriented along the  $O_c$ –Al direction, with a negligible contribution from the AOs of Al atoms. Two similar WFs are associated to the  $O_d$  ( $\omega_d^{1o}, \omega_d^{2o}$ ), and lone pair ( $\omega_d^{1o}$ ) and bond ( $\omega_d^h$ ) WFs are present as a result of the combination of the p-type AOs of  $O_d$  with the AOs of the close H atoms. The same type of WFs can be found on  $\mathcal{D}s$  with a different distribution. In  $\mathcal{D}s$  both symmetry-inequivalent O atoms have three Al atoms as first neighbors, so they both have three *atomic* WFs ( $\omega_a^1, \omega_a^2, \omega_a^3$  and  $\omega_b^1, \omega_b^2, \omega_b^3$ ), but  $O_a$  is the HB acceptor and  $O_b$  is directly linked to the H atom, so that the lone-pair WF is located on  $O_a$  ( $\omega_a^{1o}$ ) while the O–H bond WF is localized on  $O_b$  ( $\omega_b^h$ ).

In Table 6 different partitions of the correlation energy are presented. Summing the contributions  $E_{ij}^{(2)}$  for WW pairs (i) with the lattice index of the second WF  $J$  running from zero up to a crystal cell closer than  $d = 12$  Å to the reference cell and (ii) considering only WFs centered on the same (or symmetry-equivalent) atom,  $\omega_i, \omega_j \in O_x$  (with  $x = a, b, c, d$ ), we end with a difference between the two monohydroxides of +0.2 kJ/mol in favor of the layered compound. Despite their high absolute values, these contributions, dominated by the strong WW pairs,

**Table 6. Partition of the Correlation Energy in Terms of Different WW Pair Contributions (see text for details)<sup>a</sup>**

(ij) $\mathcal{D}s$	$E_{ij}^{(2)}$	(ij) $\mathcal{B}h$	$E_{ij}^{(2)}$	$\Delta E_{ij}^{(2)}[\mathcal{D}s - \mathcal{B}h]$
$O_a$	−981.1	$O_c$	−970.3	
$O_b$	−961.6	$O_d$	−972.6	
$\sum_{ij}$	−1942.7	$\sum_{ij}$	−1942.9	+0.2
$\omega_b^2 - \omega_b^1$	−10.7	$\omega_c^1 - \omega_c^2$	−1.7	
$\omega_b^2 - \omega_a^1$	−28.4	$\omega_c^1 - \omega_d^1$	−25.1	
$\omega_b^2 - \omega_a^{1o}$	−8.7	$\omega_c^1 - \omega_d^{1o}$	−8.3	
$\omega_a^1 - \omega_a^{1o}$	−7.5	$\omega_d^{1o} - \omega_d^1$	−7.2	
$\omega_a^1 - \omega_b^h$	−6.5	$\omega_c^1 - \omega_d^h$	−4.2	
$\omega_b^2 - \omega_b^h$	−5.1	$\omega_d^{1o} - \omega_d^{1o}$	−6.2	
$\omega_a^{1o} - \omega_b^h$	−13.1	$\omega_d^{1o} - \omega_d^h$	−10.8	
$\sum_{ij}$	−80.0		−63.5	−16.5

<sup>a</sup>Energies are in kJ/mol per  $\text{Al}_2\text{O}_3$ .

are not the main responsible for the relative energy between the monohydroxides because they cancel nearly exactly when the energy difference is computed.

On the contrary, the other contributions listed in Table 6, referring to pairs for which (i) the  $J$  lattice vector index can run up to  $d = 12$  Å and (ii) the two WFs are centered on different atoms,  $\omega_i \in O_x, \omega_j \in O_y$ , regardless of their lower absolute value, favor the  $\mathcal{D}s$  phase and are responsible for its higher stability with respect to the layered structure. In particular, the HB correlation energy, pairs  $\omega_a^{1o} - \omega_b^h$  and  $\omega_d^{1o} - \omega_d^h$ , is stronger for  $\mathcal{D}s$ , and also the dispersion contributions due to atomic WFs,  $\omega_b^2 - \omega_a^1, \omega_b^2 - \omega_b^1$  and  $\omega_c^1 - \omega_d^1, \omega_c^1 - \omega_c^2$ , tend to stabilize  $\mathcal{D}s$ . The overall effect is around −16.5 kJ/mol which is almost the energy gained when WW pairs in a sphere of 3.0 Å around the reference cell are considered.

In summary, the gain in energy due to the correlation of electron on the same atom (*strong* pairs) is sensitive but almost equivalent in the two structures. Short-range correlation effects between first-neighbor O atoms are responsible for the lower  $\mathcal{D}s$  energy, and the presence of a lone pair and an O–H bond on the same atom ( $\mathcal{B}h$ ) appears a less favorable configuration.

## 4. CONCLUSIONS

The relative energy of Al mono- and trihydroxides was investigated by means of the post-HF approaches as implemented in the CRYSCOR code. These systems are at the limit of the current capability of the code in terms of size and consequently an accurate calibration of the computational setting was necessary to achieve reliable results.

LMP2 is capable of predicting relative energies in agreement with experimental data, and it is able to quantitatively determine the contribution of electron correlation. Minor structural differences obtained when optimizing with different DFT functionals turn out to be negligible when both the short- and long-range correlation effects are correctly taken into account. Actually, a more accurate description of dispersive forces seems to be the key to allow for a more accurate set of relative energies.

A tentative interpretation of the relative energy of monohydrates is given in terms of short-range correlation effects between oxygen atoms, whose electronic structure is more favorable for  $\mathcal{D}s$  than for  $\mathcal{B}h$ . In particular, the partition of the correlation contribution in terms of distance and type of occupied orbitals shows the importance of an accurate description of the correlation between electrons belonging to



509 first-neighbor O atoms in deciding the stability between  
510 monohydroxides.

511 A new minimum energy structure (ST2) was obtained when  
512 optimizing  $N$  with the PBE0 functional. The  $c$  and  $\alpha$  lattice  
513 parameters are 9–15% smaller than those proposed as a result  
514 of experimental and previous computational studies (ST1).  
515 Although ST1 geometry and energy are in better agreement  
516 with the few available experiments, we cannot exclude ST2  
517 from being a candidate to describe the  $N$  structure, because it  
518 is  $\approx 15$  kJ/mol per  $\text{Al}_2\text{O}_3$  unit more stable than ST1. However,  
519 this shows also that  $\text{Al}(\text{OH})_3$  polymorphs have versatile  
520 structures, exhibiting various possible arrangements of the HB  
521 pattern and of the structural parameters related to the stacking  
522 of the layers and thus leading to the presence of additional  
523 minima on the energy hypersurface.

## 524 ■ AUTHOR INFORMATION

### 525 Corresponding Author

526 \*E-mail: [silvia.casassa@unito.it](mailto:silvia.casassa@unito.it).

### 527 Notes

528 The authors declare no competing financial interest.

## 529 ■ ACKNOWLEDGMENTS

530 The authors thank Cineca (grant HP10BGUEON), iVEC, and  
531 National Computational Infrastructure, Australia, for providing  
532 computing resources, as well as Roberto Dovesi for careful  
533 reading, comments, and suggestions.

## 534 ■ REFERENCES

- 535 (1) Wefers, K.; Misra, C. Oxydes and hydroxides of aluminium,  
536 Technical Report 19, ALCOA Laboratories, Pittsburgh, PA, 1987.  
537 (2) Gitzen, W. H. *Alumina as a ceramic material*; American Ceramic  
538 Society: Westerville, OH, 1970.  
539 (3) Wefers, K. *Nomenclature, preparation, and properties of aluminium*  
540 *oxide hydroxides, and trihydroxides*; Vol. Alumina Chemicals: Science  
541 and Technology Handbook; Hart, L. D., Ed.; American Ceramic  
542 Society: Westerville, OH, 1990; pp 13–22.  
543 (4) Trueba, M.; Trasatti, S. P. *Eur. J. Inorg. Chem.* **2005**, *17*, 3393–  
544 3403.  
545 (5) Musselman, L. L. *Production processes, properties, and applications*  
546 *for aluminium-containing hydroxides*; Vol. Alumina Chemicals: Science  
547 and Technology Handbook; Hart, L. D., Ed.; American Ceramic  
548 Society: Westerville, OH, 1990; pp 72–92.  
549 (6) Merck. *The Merck Manual Online Technical Report*; Merck Sharp  
550 & Dohme Corp.: Whitehouse Station, NJ, 2004–2010.  
551 (7) Demichelis, R.; Noël, Y.; Ugliengo, P.; Zicovich-Wilson, C. M.;  
552 Dovesi, R. *J. Phys. Chem. C* **2011**, *115*, 13107–13134.  
553 (8) Gale, J. D.; Rohl, A. L.; Milman, V.; Warren, M. C. *J. Phys. Chem.*  
554 *B* **2001**, *105*, 10236–10242.  
555 (9) Noël, Y.; Demichelis, R.; Ugliengo, P.; Pascale, F.; Orlando, R.;  
556 Dovesi, R. *Phys. Chem. Miner.* **2009**, *36*, 47–59.  
557 (10) Winkler, B.; Hytha, M.; Pickard, C.; Milman, V.; Warren, M. C.;  
558 Segall, M. *Eur. J. Mineral.* **2001**, *13*, 343–349.  
559 (11) Frenzel, J.; Oliveira, A. F.; Duarte, H. A.; Heine, T.; Seifert, G. Z.  
560 *Anorg. Allg. Chem.* **2005**, *631*, 1267–1271.  
561 (12) Demichelis, R.; Civalleri, B.; Noël, Y.; Meyer, A.; Dovesi, R.  
562 *Chem. Phys. Lett.* **2008**, *465*, 220–225.  
563 (13) Demichelis, R.; Catti, M.; Dovesi, R. *J. Phys. Chem. C* **2009**, *113*,  
564 6785–6791.  
565 (14) Wang, S. L.; Johnston, C. T. *Am. Mineral.* **2000**, *85*, 739–744.  
566 (15) Balan, E.; Lazzeri, M.; Morin, G.; Mauri, F. *Am. Mineral.* **2006**,  
567 *91*, 115–119.  
568 (16) Balan, E.; Blanchard, M.; Hochepied, J. F.; Lazzeri, M. *Phys.*  
569 *Chem. Miner.* **2008**, *35*, 279–285.

- (17) Demichelis, R.; Noël, Y.; Civalleri, B.; Roetti, C.; Ferrero, M.;  
Dovesi, R. *J. Phys. Chem. B* **2007**, *111*, 9337–9346.  
(18) Raybaud, P.; Digne, M.; Iftimie, R.; Wellens, W.; Euzen, P.;  
Toulhoat, H. *J. Catal.* **2001**, *201*, 236–246.  
(19) Digne, M.; Sautet, P.; Raybaud, P.; Euzen, P.; Toulhoat, H. *J.*  
*Catal.* **2002**, *211*, 1–5.  
(20) Digne, M.; Sautet, P.; Raybaud, P.; Toulhoat, H.; Artacho, E. *J.*  
*Phys. Chem. B* **2002**, *106*, 5155–5162.  
(21) Wolverton, C.; Hass, K. C. *Phys. Rev. B* **2001**, *63*, 024102.  
(22) Rosso, K. M.; Rustad, J. R. *Am. Mineral.* **2001**, *86*, 312–317.  
(23) Krokidis, X.; Raybaud, P.; Gobichon, A. E.; Rebours, B.; Euzen,  
P.; Toulhoat, H. *J. Phys. Chem. B* **2001**, *105*, 5121–5130.  
(24) Demichelis, R.; Civalleri, B.; D'Arco, P.; Dovesi, R. *Int. J.*  
*Quantum Chem.* **2010**, *110*, 2260–2273.  
(25) Verdes, G.; Gout, R.; Castet, S. *Eur. J. Mineral.* **1992**, *4*, 767–  
792.  
(26) Parks, G. A. *Am. Mineral.* **1972**, *57*, 1163–1189.  
(27) Lide, D. R. *Handbook of chemistry and physics*; CRC Press: Boca  
Raton, FL, 1991–1992.  
(28) Hemingway, B. S.; Sposito, G. Inorganic aluminium-bearing  
solid phases. In *The environmental chemistry of aluminium*; Sposito, G.,  
Eds.; CRC Press: Boca Raton, 1995; pp 81–116.  
(29) Ogorodovaa, L. P.; Kiselevaa, I. A.; Sokolovab, E. L.; Vigasinaa,  
M. F.; Kabalova, Y. K. *Geochem. Int.* **2012**, *50*, 90–94.  
(30) Milman, B. W. V.; Hennion, B.; Payne, M. C.; Lee, M. H.; Lin, J.  
*S. Phys. Chem. Miner.* **1995**, *22*, 461–467.  
(31) Pulay, P. *Chem. Phys. Lett.* **1983**, *100*, 151–154.  
(32) Pulay, P.; Saebo, S. *Theor. Chim. Acta* **1986**, *69*, 357–368.  
(33) Saebo, S.; Pulay, P. *J. Chem. Phys.* **1987**, *86*, 914–922.  
(34) Pisani, C.; Busso, M.; Capecchi, G.; Casassa, S.; Dovesi, R.;  
Maschio, L.; Zicovich-Wilson, C. M.; Schütz, M. *J. Chem. Phys.* **2005**,  
*122*, 094144.  
(35) Cryscor User's Manual. Erba, A.; Halo, M.; [www.cryscor.unito.it](http://www.cryscor.unito.it), 2009.  
(36) CRYSTAL 2009 User's Manual. Dovesi, R.; Saunders, V. R.;  
Roetti, C.; Orlando, R.; Zicovich-Wilson, C. M.; Pascale, F.; Civalleri,  
B.; Doll, K.; Harrison, N. M.; Bush, I. J.; D'Arco, P.; Llunell, M. 2009.  
(37) Pisani, C.; M, S.; Casassa, S.; Usvyat, D.; Maschio, L.; Lorenz,  
M.; Erba, A. *Phys. Chem. Chem. Phys.* **2012**, *14* (21), 7615–7628.  
(38) Maschio, L. *J. Chem. Theory Comput.* **2011**, *7* (9), 2818–2830.  
(39) Slater, J. C. *Phys. Rev.* **1951**, *81*, 385–390.  
(40) Vosko, S. H.; Wilk, L.; Nusair, M. *Can. J. Phys.* **1980**, *58*, 1200–  
1211.  
(41) Perdew, J. P.; Burke, K.; Ernzerhof, M. *Phys. Rev. Lett.* **1996**, *77*,  
3865–3868.  
(42) Perdew, J.; Ruzsinsky, A.; Csonka, G. I.; Vydrov, O. A.; Scuseria,  
G. E.; Constantin, L. A.; Zhou, X.; Burke, K. *Phys. Rev. Lett.* **2008**, *100*,  
136406.  
(43) Adamo, C.; Barone, V. *J. Chem. Phys.* **1999**, *110*, 6158–6170.  
(44) Becke, A. D. *J. Chem. Phys.* **1993**, *98*, 5648–5652.  
(45) Lee, C.; Yang, W.; Parr, R. G. *Phys. Rev. B* **1988**, *37*, 785–789.  
(46) Broyden, C. G. *J. Inst. Math. Appl.* **1970**, *6*, 76–90.  
(47) Fletcher, R. *Comput. J.* **1970**, *13*, 317–322.  
(48) Goldfarb, D. *Math. Comput.* **1970**, *24*, 23–26.  
(49) Shanno, D. F. *Math. Comput.* **1970**, *24*, 647–656.  
(50) Zicovich-Wilson, C. M.; Dovesi, R. *Int. J. Quantum Chem.* **1998**,  
*67*, 299–309.  
(51) S. Casassa, C. M. Z.-W.; Pisani, C. *Theor. Chem. Acc.* **2006**, *116*,  
726.  
(52) Demichelis, R.; Civalleri, B.; Ferrabone, M.; Dovesi, R. *Int. J.*  
*Quantum Chem.* **2010**, *110*, 406–415.  
(53) Pisani, C.; Maschio, L.; Casassa, S.; Halo, M.; Schütz, M.;  
Usvyat, D. *J. Comput. Chem.* **2008**, *29*, 2113–2124.  
(54) Schütz, M.; Usvyat, D.; Lorenz, M.; Pisani, C.; Maschio, L.;  
Casassa, S.; Halo, M. Density fitting for correlated calculations in  
periodic systems. In *Accurate Condensed Phase Quantum Chemistry*;  
Manby, F. R., Ed.; CRC Press: Boca Raton, 2010; pp 29–56.  
(55) Dunning, T. H. *J. Chem. Phys.* **1989**, *90*, 1007–1023.

- 638 (56) Dunning, T. H.; Peterson, K. A.; Wilson, A. K. *J. Chem. Phys.*  
639 **2001**, *114*, 9244–9253.
- 640 (57) Saalfeld, H.; Jarchow, O. *Neues Jahrb. Mineral.* **1968**, *109*, 185–  
641 191.
- 642 (58) Chao, G. Y.; Baker, J. *Can. Mineral.* **1982**, *20*, 77–85.